Ocean Eddy Dynamics in a Coupled Ocean–Atmosphere Model*

P. BERLOFF

Physical Oceanography Department, Woods Hole Oceanographic Institution, Woods Hole, Massachusetts, and Department of Applied Mathematics and Theoretical Physics, University of Cambridge, Cambridge, United Kingdom

W. DEWAR

Department of Oceanography, The Florida State University, Tallahassee, Florida

S. KRAVTSOV

Department of Mathematical Sciences, University of Wisconsin—Milwaukee, Milwaukee, Wisconsin

J. MCWILLIAMS

Department of Atmospheric and Oceanic Sciences, University of California, Los Angeles, Los Angeles, California

(Manuscript received 14 June 2005, in final form 27 June 2006)

ABSTRACT

The role of mesoscale oceanic eddies is analyzed in a quasigeostrophic coupled ocean–atmosphere model operating at a large Reynolds number. The model dynamics are characterized by decadal variability that involves nonlinear adjustment of the ocean to coherent north–south shifts of the atmosphere. The oceanic eddy effects are diagnosed by the dynamical decomposition method adapted for nonstationary external forcing. The main effects of the eddies are an enhancement of the oceanic eastward jet separating the subpolar and subtropical gyres and a weakening of the gyres. The flow-enhancing effect is due to nonlinear rectification driven by fluctuations of the eddy forcing. This is a nonlocal process involving generation of the eddies by the flow instabilities in the western boundary current and the upstream part of the eastward jet. The eddies are advected by the mean current to the east, where they backscatter into the rectified enhancement of the eastward jet. The gyre-weakening effect, which is due to the time-mean buoyancy component of the eddy forcing, is a result of the baroclinic instability of the westward return currents. The diagnosed eddy forcing is parameterized in a non-eddy-resolving ocean model, as a nonstationary random process, in which the corresponding parameters are derived from the control coupled simulation. The key parameter of the random process—its variance—is related to the large-scale flow baroclinicity index. It is shown that the coupled model with the non-eddy-resolving ocean component and the parameterized eddies correctly simulates climatology and low-frequency variability of the control eddy-resolving coupled solution.

1. Introduction

We study the dynamic role of the mesoscale oceanic eddies in an idealized coupled ocean–atmosphere model of midlatitude climate (Kravtsov et al. 2006, 2007). The model components are placed in a highly nonlinear regime by an appropriate choice of spatial resolution and frictional parameters and are characterized by vigorous intrinsic variability. The oceanic flow is in the classical double-gyre circulation regime, which has been considered previously with prescribed wind forcing. Here, the ocean is forced by and can feed back on the dynamically evolving atmosphere. Our goals are to analyze the oceanic mesoscale eddy effects on the large-scale circulation and to develop a stochastic eddy parameterization for use in a coupled model with a non-eddy-resolving ocean component.

In this section we provide some background, pose the

* Woods Hole Oceanographic Institution Contribution Number 11387.

Corresponding author address: P. Berloff, Physical Oceanography Dept., Woods Hole Oceanographic Institution, Woods Hole, MA 02543.
E-mail: pberloff@whoi.edu

DOI: 10.1175/JPO3041.1

problem, and describe the coupled model. The climatology and the low-frequency variability of the reference solution, as well as the diagnostics of the eddy forcing are described in section 2. The eddy effects on the large-scale flow are analyzed and discussed in section 3. The eddy parameterization is formulated and tested in section 4, and the results are summarized in section 5.

a. Background

The observed decadal variability in the midlatitude ocean and atmosphere (e.g., Wallace 2000; Deser and Blackmon 1993; Kushnir 1994) can be explained in terms of either intrinsic variabilities of the ocean and atmosphere or as a coupled ocean–atmosphere phenomenon. Coupled ocean–atmosphere general circulation models (GCMs) do not yet discriminate between these alternatives: some models suggest that the coupling is important (e.g., Latif and Barnett 1994) while the others do not (e.g., Pierce et al. 2001). It is thus sensible to analyze idealized coupled and uncoupled models in order to get insight into potential mechanisms of the observed low-frequency variability. Recent advances in understanding coupled dynamics have been made with midlatitude, quasigeostrophic models that resolve mesoscale turbulence in both the oceanic and atmospheric components (Hogg et al. 2003; Kravtsov et al. 2006, 2007; Hogg et al. 2005, 2006). Kravtsov et al. (2006, 2007) have shown that atmospheric transitions between the pair of statistically preferred states and the nonlinear adjustment of the ocean (Dewar 2003) to these states can be the essential mechanisms of decadal coupled variability. An important point is that the oceanic adjustment is controlled by the mesoscale eddies. If the eddies are parameterized in terms of eddy viscosity, coupled variability is suppressed. This is presumably because the physical process, by which the eddies maintain sea surface temperature anomalies feeding back on the atmosphere, is not fundamentally a viscous one.

Although the role of oceanic mesoscale eddies in shaping the large-scale ocean circulation has been known for a long time (e.g., Holland 1978), accurate mathematical models (i.e., parameterizations) of the eddy effects are not yet generally available for use in non-eddy-resolving GCMs. The most common eddy parameterization, which in different forms is present in virtually all GCMs, is eddy viscosity (Taylor 1921). However, when the large-scale currents are enhanced rather than smoothed by the eddies, such parameterizations can be incorrect. Such situations are common in geophysical flows (Starr 1968). Progress in simulating "negative viscosity" has been made in terms of random forcing added to an otherwise non-eddy-resolving ocean model (Berloff 2005b). This approach falls into a broad class of fluid dynamic models in which the small-scale nonlinear interactions are replaced by stochastic processes (e.g., Herring and Kraichnan 1971). Other eddy models are based on representation of the eddies by ensembles of particles advected by and interacting with the large-scale flow (Laval et al. 2003), or on the assumption that the eddies are passively advected by the large-scale flow (Holm and Nadiga 2003).

b. Statement of the problem

The main goals of the present paper are to diagnose and understand the oceanic mesoscale eddy effects in an idealized ocean–atmosphere coupled model (Kravtsov et al. 2006, 2007) and to develop a stochastic parameterization of these eddy effects for use in a coupled model with a non-eddy-resolving ocean component. The following specific steps are made. First, the history of the eddy forcing is diagnosed from the eddy-resolving solution and then analyzed statistically and dynamically. The mechanism of the eddy/mean flow interaction is uncovered, and the effects of the eddies on the large-scale flow are separated from the effect of the wind. Statistics of the eddy forcing are treated as nonstationary, because the coupled solution is characterized by significant decadal variability.

Next, in a non-eddy-resolving ocean component of the coupled model, eddy forcing is simulated as a stochastic, space–time correlated process with spatially inhomogeneous variance. It is found that imposed stationarity of the random-forcing variance suppresses the low-frequency variability but has small impact on the climatology. On the other hand, the low-frequency variability is recovered if the parameterization allows for nonstationarity of the eddy-forcing variance. This is achieved by relating the variance to the large-scale flow, and amounts to a simple parameter closure. The random forcing is ultimately related to the large-scale flow, thus yielding a closed stochastic model of the eddy effects.

The problem is posed so that statistics (i.e., parameters) of the random-forcing parameterization come from the reference eddy-resolving solution. Here, the goals pursued are to identify the appropriate mathematical model for and the relevant physics behind future parameterizations. A related, if distinct, result of this paper is the illustration of a *systematic strategy* for developing eddy parameterization that can be employed in a hierarchy of eddy-resolving models, from idealized to comprehensive. Our ultimate result is close to an internally closed parameterization in that the implementation of the parameterization is related in a

TABLE 1. Table of the frequently used symbolic notations. Index $i = \overline{1,3}$ indicates isopycnal layer.

Notation	Quantity
Ψ_i	Velocity streamfunction of the eddy-resolving (ER) solution
Q_i	Potential vorticity anomaly of the ER solution
ψ_i, q_i	Velocity streamfunction and the corresponding potential vorticity anomaly of the ER solution projected on the coarse grid
$\overline{\psi_i}$, $\overline{q_i}$	Large-scale components of ψ_i and q_i
ψ_i^*, q_i^*	Eddy components of ψ_i and q_i
f_i	Eddy forcing
R_i	Relative vorticity component of f_i
B_i	Buoyancy component of f_i
$\langle A \rangle$	Time-mean component of some quantity $A(t)$
A'	Fluctuation component of $A(t)$
$\sigma(A)$	Variance of $A(t)$
$\{A\}$	Conditional average of the ensemble of states A
$\Sigma(A)$	Conditional variance of the ensemble of states A
W	Total atmospheric forcing of the ocean
K	Kinetic energy conversion term
Π	Potential energy conversion term
I^A_{BT}	Barotropic atmospheric index
I^O_{BT}	Barotropic oceanic index
I^O_{BC}	Baroclinic oceanic index
I^O_f	Eddy-forcing index
$\mathrm{EJ} - I^O_{\mathrm{L1}}$	Oceanic eastward-jet index

self-consistent way to a measure of the ocean state. On the other hand, we stop short of developing a fully closed parameterization because details of the parameterization are diagnosed from an analysis of an eddy-resolving run. It is our hope ultimately to complete the closure, but in these early days of experimentation with stochastic closures, the demonstration of their utility represents a significant contribution.

c. Coupled model

The coupled model consists of a closed rectangular 5120 km × 5600 km ocean basin and an overlying zonally periodic 20 480 km × 6400 km atmospheric channel on the beta plane (Kravtsov et al. 2006). Both oceanic and atmospheric components are quasigeostrophic, with two isopycnal layers (H_{1a} = 3000 m and H_{2a} = 7000 m) in the atmosphere and three isopycnal layers (H_1 = 300, H_2 = 700, and H_3 = 3000 m) in the ocean. The interior ocean and the atmosphere are coupled through a 50-m-deep oceanic mixed layer, in which sea surface temperature (SST) is advected by both geostrophic and Ekman currents. The SST and the atmosphere are connected by surface heat exchange. The atmospheric model's parameters are as in experiment 2 of Kravtsov et al. (2007, their Table 1).

The ocean model's potential vorticities Q_i (index $i = \overline{1,3}$ denotes the layers) are given by

$$Q_1 = \nabla^2\Psi_1 - S_1(\Psi_1 - \Psi_2) + \beta y, \tag{1}$$

$$Q_2 = \nabla^2\Psi_2 - S_{21}(\Psi_2 - \Psi_1) - S_{22}(\Psi_2 - \Psi_3) + \beta y, \quad \text{and} \tag{2}$$

$$Q_3 = \nabla^2\Psi_3 - S_3(\Psi_3 - \Psi_2) + \beta y, \tag{3}$$

where Ψ_i are the corresponding isopycnal-layer velocity streamfunctions, and $\beta = 2 \times 10^{-11}$ m^{-1} s^{-1} is the planetary vorticity gradient. (The most common symbols are cited in Table 1.) The stratification parameters are

$$S_1 = \frac{f_0^2}{H_1 g_1'}, S_{21} = \frac{f_0^2}{H_2 g_1'}, S_{22} = \frac{f_0^2}{H_2 g_2'}, \quad \text{and} \quad S_3 = \frac{f_0^2}{H_3 g_2'}, \tag{4}$$

where $g_1' = 0.042$ m s^{-2} and $g_2' = 0.022$ m s^{-2} are reduced gravities, associated with the density jumps across the upper and lower internal interfaces between the isopycnal layers, and $f_0 = 10^{-4}$ s^{-1} is the Coriolis parameter. Given (4), the first and second internal Rossby radii are equal to 46 and 26 km, respectively. Evolution of the potential vorticity anomalies is governed by

$$\frac{\partial Q_1}{\partial t} + J(\Psi_1, Q_1) = \frac{f_0}{H_1}(W_E - W_D) + \nu\nabla^4\Psi_1, \tag{5}$$

$$\frac{\partial Q_2}{\partial t} + J(\Psi_2, Q_2) = \frac{f_0}{H_2} W_D + \nu\nabla^4\Psi_2, \quad \text{and} \tag{6}$$

$$\frac{\partial Q_3}{\partial t} + J(\Psi_3, Q_3) = -\frac{1}{2} f_0 \frac{H_{\mathrm{bot}}}{H_3} \nabla^2\Psi_3 + \nu\nabla^4\Psi_3, \tag{7}$$

where $J(A, B) \equiv A_x B_y - A_y B_x$ is the Jacobian operator, H_{bot} = 30 m is the thickness of the bottom boundary layer, and ν = 200 m^2 s^{-1} is the horizontal viscosity coefficient. The forcing consists of a time-dependent Ekman pumping W_E and heat exchange W_D between the ocean interior and mixed layer (the latter is a crude parameterization of the meridional overturning circulation). Both of these quantities are diagnostically related to the states of the atmosphere and mixed layer. Equations (5)–(7), subject to partial-slip conditions on the lateral boundaries and mass conservation (McWilliams 1977), are discretized on a 513 × 561, 10-km-resolution grid and integrated using leapfrog time stepping with a 20-min interval.

2. Coupled ocean–atmosphere solution

a. Climatology and low-frequency variability

The eddy-resolving coupled solution, calculated over 400 yr, is referred to as the full *reference* solution. Its time-mean structure is shown in Fig. 1. The ocean is

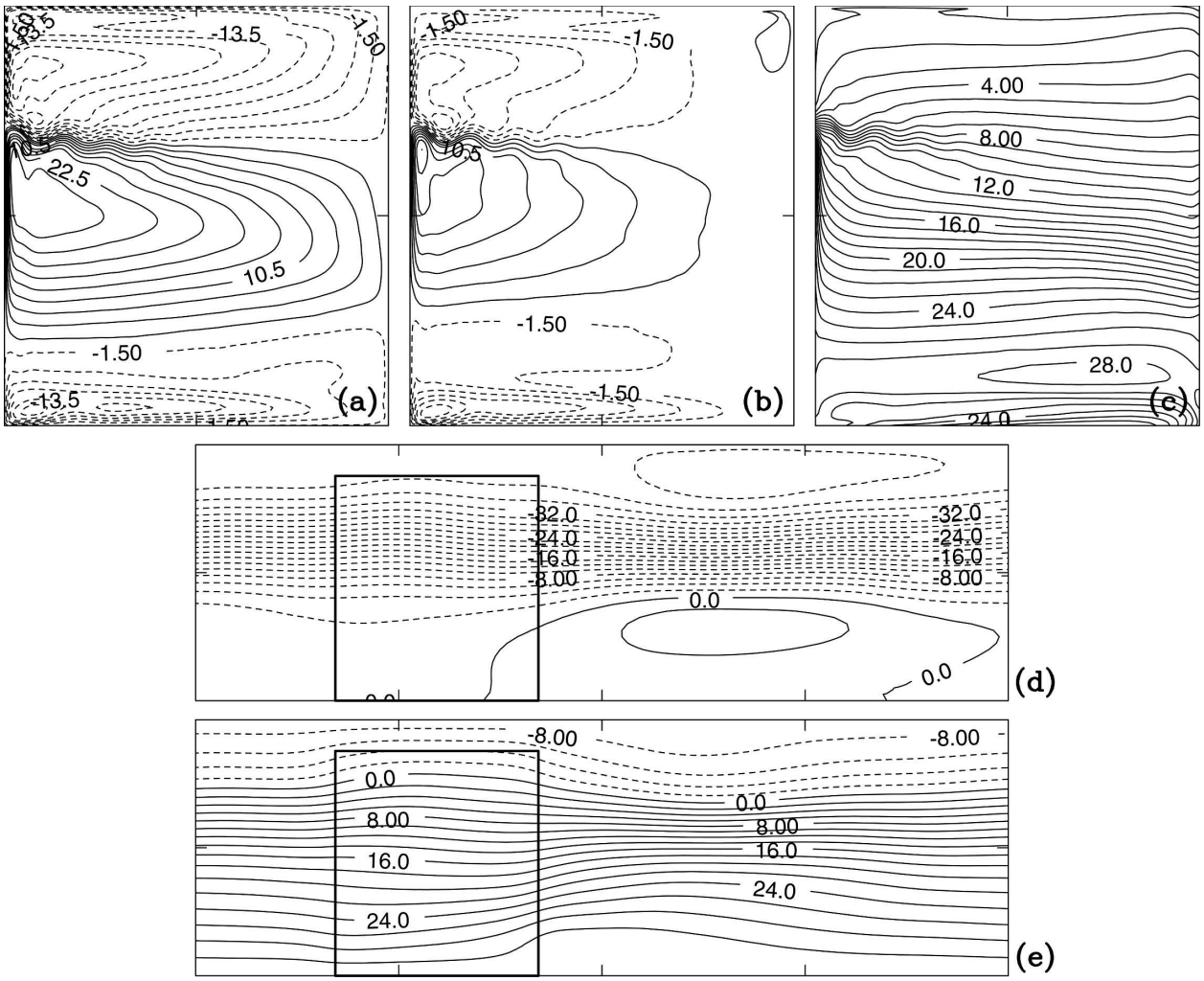

FIG. 1. Climatology of the eddy-resolving reference solution of the coupled ocean–atmosphere model (Kravtsov et al. 2005): (a)–(c) ocean and (d), (e) atmosphere. Time-mean velocity streamfunctions in the (a) upper (ψ_1) and (b) deep (ψ_2) ocean [contour interval (CI) = 3 Sv (1 Sv $\equiv 10^6$ m^3 s^{-1})], and the corresponding (c) time-mean sea surface temperature (CI = 1°C). Time-mean (d) barotropic velocity streamfunction of the atmosphere (CI = 2×10^6 m^2 s^{-1}) and (e) temperature (CI = 1°C). The ocean basin is outlined in (d) and (e).

dominated by subtropical and subpolar gyres of unequal strengths. The gyres are separated by the eastward-jet extension of the pair of merging western boundary currents. The axis of the eastward jet coincides with a sharp SST front. With depth, the gyres weaken and retreat to the western boundary. There is also a third, southern gyre, but it is relatively weak. The atmospheric component of the model is dominated by an eastward jet with a reasonable storm track and meridional temperature profile. In the ocean, the time-mean Ekman pumping, W_E, is strongly dependent on longitude as well as latitude (Fig. 2). The time-mean thermodynamic forcing, W_D, is set to zero through iterative corrections (Kravtsov et al. 2006).

The low-frequency variability of the reference solution around its time-mean state is analyzed with empirical orthogonal function (EOF) decomposition (Preisendorfer 1988). It is found that the atmospheric variability is dominated by zonally shifting winds (Fig. 3), and the corresponding leading EOF accounts for about half of the variances of W_E and W_D. The three leading oceanic EOFs contain about ⅔ of the total oceanic variance, with the first EOF accounting for nearly half (Fig. 4). The first EOF describes irregular but roughly decadal transitions of the ocean between a more preferred low-latitude state and a more transient high-latitude state. These states correspond to positive and negative values of the first principal component (Fig. 4d). The most dramatic transitions to the low-latitude state are associated with shifts of the eastward-jet

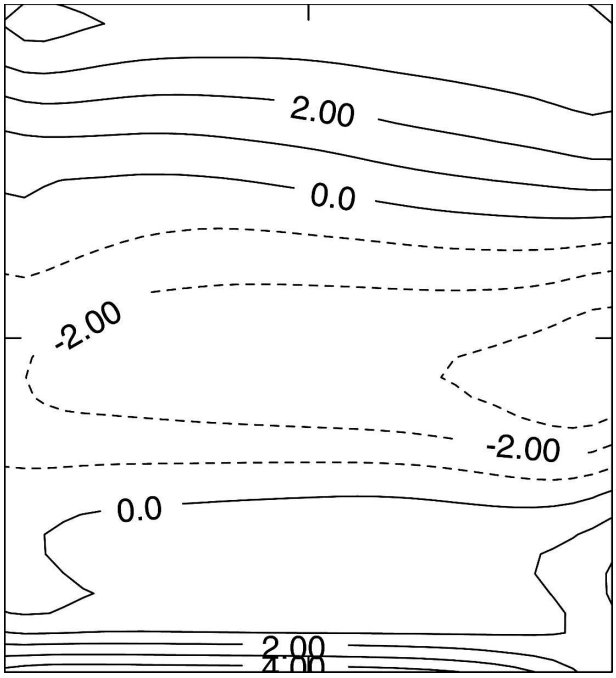

FIG. 2. Time-mean Ekman pumping W_E (CI = 10^{-6} m s^{-1}).

axis by a few hundred kilometers to the south. As shown by Kravtsov (2007), the transition time scale is set by the nonlinear adjustment of the ocean. The principal components of the second and third EOFs are time-lag correlated; thus they describe a westward propagating signal with a 4-yr period. This signal is identified in Kravtsov et al. (2006, 2007) to be a first baroclinic basin mode amplified by coupling with the atmosphere (Goodman and Marshall 1999).

b. Diagnostics of the eddies

The dynamical eddy analysis (Berloff 2005a), generalized to allow for time-dependent external forcing of the ocean, is now applied. The reference ocean solution is projected on a uniform 129 × 141, 40-km-resolution grid by subsampling all three layer streamfunctions in both space and time, the latter at an interval of 5 days. The goal is to decompose the projected reference solution, denoted by ψ_i and q_i, as

$$\begin{aligned}\psi_i(t,x,y) &= \overline{\psi_i}(t,x,y) + \psi_i^*(t,x,y), q_i(t,x,y)\\ &= \overline{q_i}(t,x,y) + q_i^*(t,x,y),\end{aligned} \tag{8}$$

where overbar and asterisk denote large-scale and eddy components of the flow, respectively. Here, potential vorticity components are found from the streamfunction according to (5)–(7). Continuous time series of both ψ_i and the forcing, $W = (W_E, W_D)$, are obtained by cubic interpolation in time. The history of W is then used to force a non-eddy-resolving ocean model, which has the same form as (5)–(7), with the addition of an eddy-forcing term as discussed below. The non-eddy-resolving model is discretized on the coarse 40-km grid; it has a horizontal viscosity[1] $\nu = 4000$ m^2 s^{-1}, and it is integrated using an 80-min time step. The additional eddy-forcing term is calculated interactively, on each time step of the non-eddy-resolving model, in terms of the difference between the non-eddy-resolving and the projected reference solutions. In each isopycnal layer, the eddy forcing is found as

$$\begin{aligned}f_i = (t,x,y) &= J(\overline{\psi_i}, \overline{q_i}) - J(\psi_i, q_i)\\ &= \nabla\cdot\overline{\mathbf{u}_\mathbf{i}}\,\overline{q_i} - \nabla\cdot\mathbf{u}_i q_i = -\nabla\cdot\mathbf{F}_i,\end{aligned} \tag{9}$$

where $J()$ and ∇ are coarse-grid operators, $\mathbf{u}_i$ is the isopycnal-layer velocity vector, and $\mathbf{F}_i$ is the effective eddy potential vorticity flux. Both the eddies and the eddy forcing are found simultaneously and interactively by integrating the eddy-corrected non-eddy-resolving model. The large-scale component of the reference flow, $\overline{\psi_i}$, is defined as the non-eddy-resolving solution, and the eddy component, ψ_i^*, is automatically found as the difference between ψ_i and $\overline{\psi_i}$. Thus, the mesoscale eddies are viewed as flow fluctuations projected on the coarse grid and dynamically accounted for by the eddy forcing. Here, the non-eddy-resolving model is initialized with $\overline{\psi_i} = \psi_i(0)$, and integrated for 400 yr. The fields of $\overline{\psi_i}$, ψ_i', and f_i are saved every 5 days.

The eddy-corrected non-eddy-resolving model captures main features of the reference solution very well (Fig. 5). When the atmospheric jet is predominantly in the low-latitude regime, the eddy forcing helps to spin up a narrow and intense oceanic eastward jet—this state is referred to as the low-latitude state of the ocean. The atmospheric high-latitude regime corresponds to the weakened oceanic eastward jet in the high-latitude state. Both states are characterized by the presence of many coherent eddies, which are analyzed in the next section.

3. Analysis of the eddy effects

a. Role of the eddies in climatology

The gross effect of the eddies on the ocean climatology is estimated by comparing the reference solution

[1] The main effect of the enhanced viscosity is limited to the viscous boundary layers, and the eddy forcing in the eastward-jet region remains largely unaffected (Berloff 2005a). In a crude way this enhancement accounts for the submesoscale eddy effects lost as a result of the coarse-grid projection of the full flow.

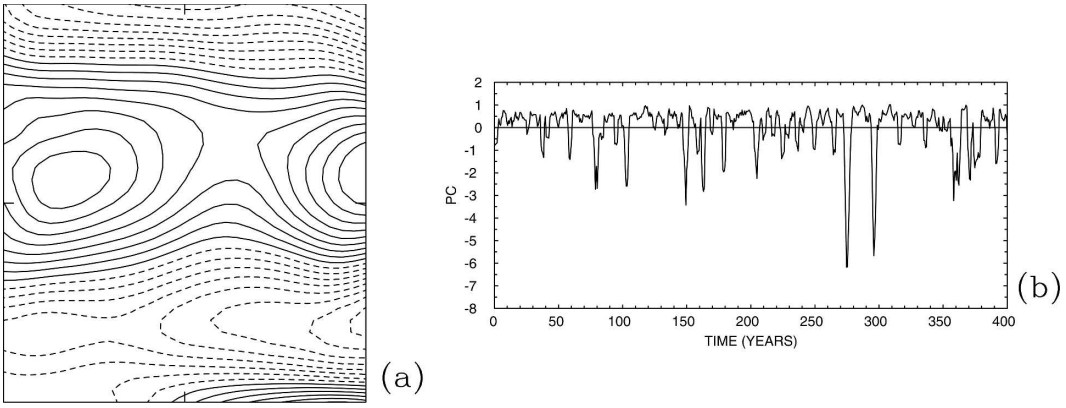

FIG. 3. The atmospheric low-frequency variability component. (a) The leading EOF of the atmospheric wind stress curl (i.e., of the Ekman pumping), shown over the ocean basin only, and (b) its principal component, low-pass filtered using a 500-day running average. The EOF is normalized by its maximum absolute value (CI = 0.1), and the principal component is normalized by its variance.

and the solution of the non-eddy-resolving model *without* the eddy forcing (Fig. 6). The latter solution has a significantly weaker eastward jet, a stronger cyclonic circulation in the northern part of the subpolar gyre, and a weaker cyclonic circulation near the southern boundary. The absence of the eastward jet results in suppression of the coupled variability (Kravtsov et al. 2006, 2007). This indicates the fundamental importance of the eddies and motivates a more detailed analysis of the eddy/large-scale flow interaction.

The eddy forcing, $f_i(t, x, y)$, diagnosed in section 2, is decomposed into time-mean, $\langle f_i \rangle(x, y)$, and fluctuating, $f_i'(t, x, y)$, components. The dynamical roles of these components can be recovered by analysis of the non-eddy-resolving ocean-only solutions forced by these components. The ocean solution forced by $W(t, x, y)$ and no f_i (Fig. 6b) has a climatology similar to that of the coupled non-eddy-resolving solution without eddy-forcing correction. The *benchmark* solution, which is driven by the time-interpolated histories of both W and f_i (Fig. 7a), is the closest approximation to the eddy-corrected non-eddy-resolving ocean solution obtained without the interpolation. Removing either $\langle f_i \rangle$ or f_i' results in a substantially different flow pattern (Figs. 7b,c). When W is imposed, effects of the eddy forcing are masked by the wind-driven gyres, but they become more evident when W is turned off (Figs. 7d–f). The strongest eddy effect is due to f_i', which is surprising because traditional analysis of the eddy effects focuses on $\langle f_i \rangle$. The f_i' effect is due to the nonlinear rectification of the flow (e.g., Haidvogel and Rhines 1983; Feliks et al. 2004; Berloff 2005b,c) by a spatially inhomogeneous eddy forcing discussed in section 3b. An important property of f_i' is its variance (Fig. 8):

$$\sigma(f_i)(x, y) = \langle f_i'^2 \rangle. \tag{10}$$

Here, it has large values in the upper ocean, and in the western boundary currents with their eastward-jet extension.

The main upper-ocean contribution of the $\langle f \rangle$ effect (i.e., the *time-mean* eddy-forcing effect) is spinning down the gyres and weakening the western boundary currents, but it is also responsible for meandering of the eastward jet (Figs. 7b,e). The former effect, which is particularly strong in the subpolar gyre, is consistent with the baroclinic instability of the westward return currents of the gyres and the western boundary currents. In terms of spinning down the gyre, the f-driven response is weaker than the sum of the $\langle f \rangle$ and f' responses, but because of the nonlinearity one should not expect any linear summation here. This nonlinear upper-ocean effect is consistent with the idea that fluctuations driven by f' tend to homogenize potential vorticity anomalies induced by $\langle f \rangle$, and thus weaken the flow response.

Analysis of the eddy forcing is extended by decomposing f_i into its relative vorticity R and buoyancy (i.e., isopycnal thickness) B components:

$$R_i = -\nabla(\overline{\mathbf{u}_i}\nabla^2\psi_i^* + \mathbf{u}_i^*\nabla^2\overline{\psi_i} + \mathbf{u}_i^*\nabla^2\psi_i^*) \quad \text{and} \tag{11}$$

$$B_i = -\nabla(\overline{\mathbf{u}_i}b_i^* + \mathbf{u}_i^*\overline{b_i} + \mathbf{u}_i^*b_i^*), \tag{12}$$

where buoyancy is

$$b_1 = -S_1(\psi_1 - \psi_2),\ b_2 = -S_{21}(\psi_2 - \psi_1) - S_{22}(\psi_2 - \psi_3),$$

and

$$b_3 = -S_3(\psi_3 - \psi_2). \tag{13}$$

The time-mean forcings, $\langle R_i \rangle$ and $\langle B_i \rangle$, induce qualitatively different flows (Fig. 9). The $\langle R \rangle$ forcing is mainly responsible for driving standing eddies that cause me-

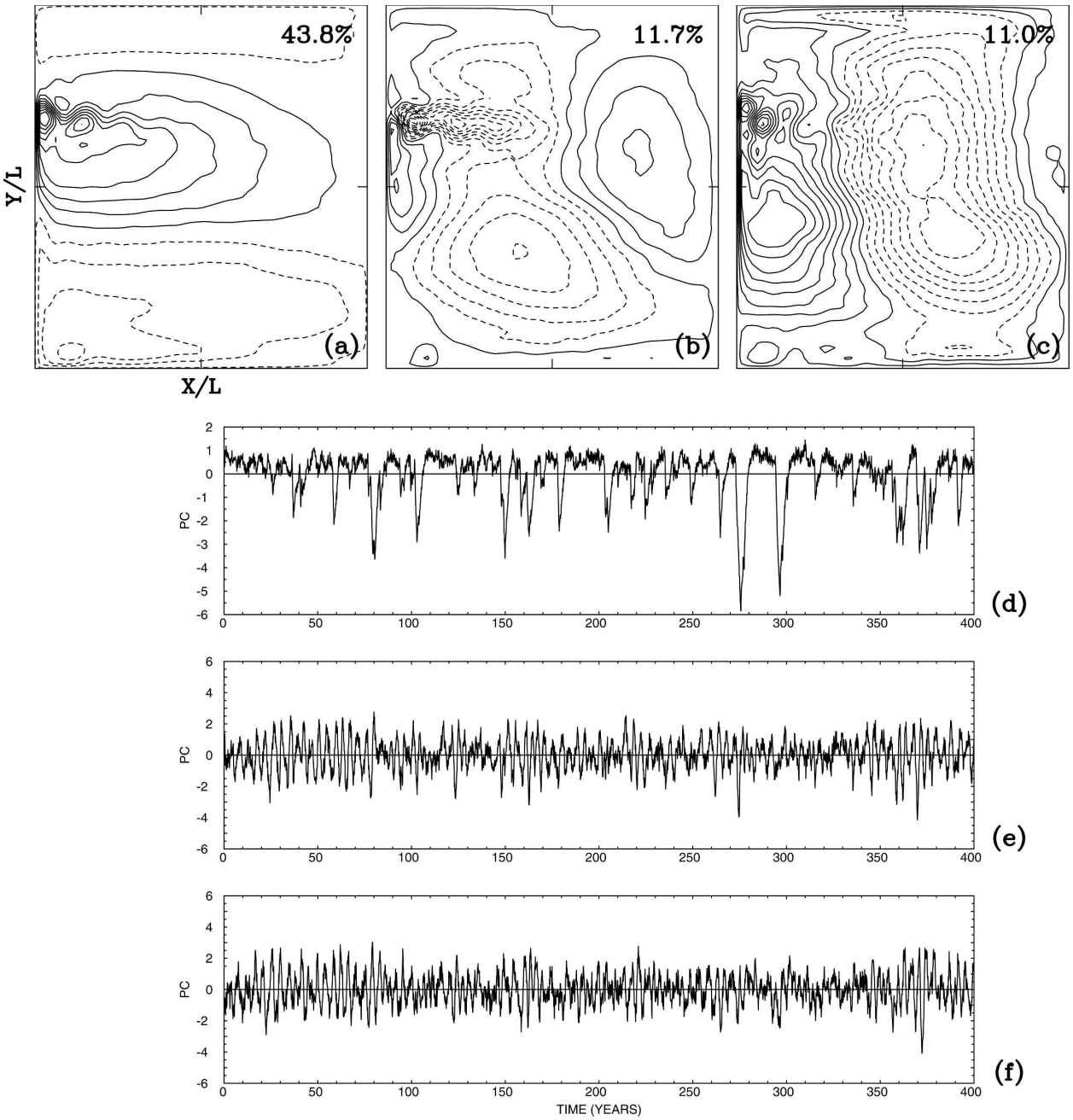

FIG. 4. The oceanic low-frequency variability component. The three leading EOFs of the upper-ocean velocity streamfunction: (a) the first, (b) the second, and (c) the third EOFs; and (d)–(f) their principal components, respectively. The corresponding fraction of the total variance is indicated in terms of percentage. The EOF is normalized by its maximum absolute value (CI = 0.1), and the principal component is normalized by its variance.

andering of the eastward jet, and its effect on the gyres is small. On the contrary, the main effect of the $\langle B \rangle$ forcing is weakening of the upper-ocean gyres, whereas its role in shaping the eastward jet is modest and opposite to that of the $\langle R \rangle$ forcing. The $\langle B \rangle$-induced pattern is consistent with the baroclinic instability of the westward flows of the gyres, and corresponds to the gyre spin down. Overall, in the eastward-jet region, the buoyancy-forcing effect is weaker than in Berloff (2005a), and the difference can be attributed to the differences in boundary conditions [no slip in Berloff (2005a) versus partial slip here] and stratification. The upper- and second-layer eddy-forcing variances are dominated by the R- and B-term contributions, respec-

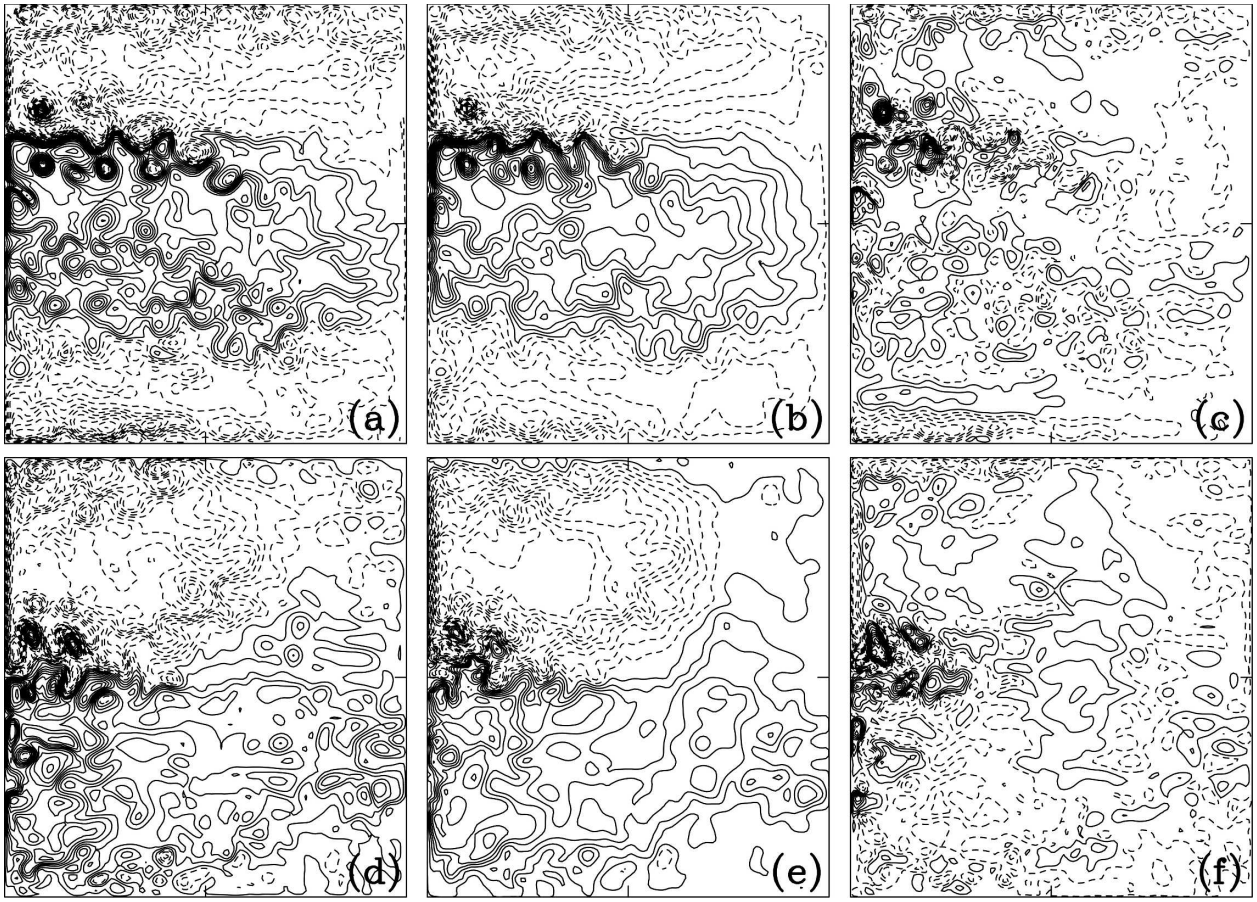

FIG. 5. Instantaneous full, large-scale, and eddy flow components (CI = 3 Sv). Flow snapshots for the low-latitude state: (a) projected reference streamfunction, $\psi_1(x, y)$, and its (b) large-scale, $\bar{\psi}_1(x, y)$, and (c) eddy, $\psi_1^*(x, y)$ components. (d)–(f) Same as in (a)–(c), but for the high-latitude state.

tively. (The second- and third-layer eddy effects are found to be qualitatively similar; therefore discussion of the deep ocean is focused on the second layer only.) This is so because the upper ocean is dominated by relatively short scale instabilities of the sharp potential vorticity front associated with the eastward jet, whereas the deep ocean is driven mostly by fluctuations in layer thicknesses, which are characterized by larger scales.

The above conclusions about the eddy-forcing components and their dynamical effects are supported by calculating the potential Π and kinetic K energy conversion terms in the conventional way (e.g., Berloff and McWilliams 1999):

$$\Pi(x, y) = -\frac{1}{2}\frac{S_1 S_{21}}{S_1 + S_{21}}\langle(\psi_1' - \psi_2')J(\psi_1' + \psi_2', \langle\psi_1\rangle - \langle\psi_2\rangle)\rangle - \frac{1}{2}\frac{S_{22} S_3}{S_{22} + S_3}\langle(\psi_2' - \psi_3')J(\psi_2' + \psi_3', \langle\psi_2\rangle - \langle\psi_3\rangle)\rangle \quad \text{and} \tag{14}$$

$$K(x, y) = -\sum_{i=1,3}\frac{H_i}{H}\left\langle\frac{\partial\psi_i'}{\partial x}J\left(\psi_i'\frac{\partial\langle\psi_i\rangle}{\partial x}\right) + \frac{\partial\psi_i'}{\partial y}J\left(\psi_i', \frac{\partial\langle\psi_i\rangle}{\partial y}\right)\right\rangle. \tag{15}$$

Here, the angle brackets denote ensemble averages and the primes denote fluctuations around these averages. The ensembles on which the averages formed are collected by conditional sampling of the model results as described below. The conversion terms are the corresponding energy exchange rates between the mean (i.e.,

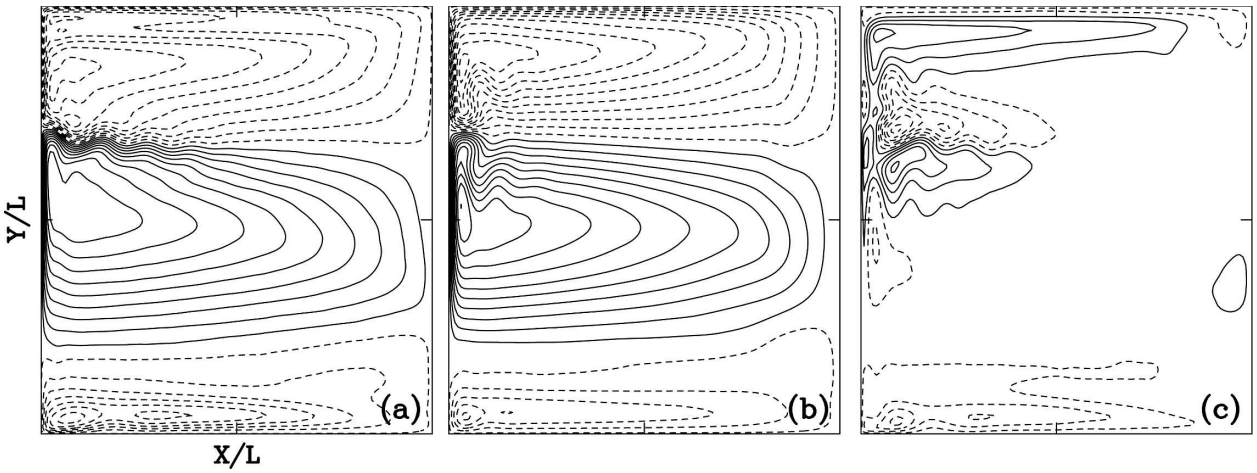

FIG. 6. The global upper-ocean effect of the eddies. Time-mean, upper-ocean velocity streamfunctions of (a) the eddy-corrected non-eddy-resolving solution; (b) the non-eddy-resolving solution that is not eddy corrected; and (c) their difference (CI = 3 Sv).

ensemble average) state and the fluctuations, which are due to the work done either by isopycnal form stresses (Π) or by horizontal Reynolds stresses (K). Barotropic instability (i.e., extracting fluctuation energy from the mean horizontal shear) is associated with a positive K, and baroclinic instability (i.e., extracting fluctuation energy from the mean vertical shear) corresponds to a positive Π. Conditional sampling is performed by defining low- and high-latitude states as occurring when the normalized principal component (PC) of EOF1 exceeds $+1$ and -1 respectively. Through ensemble averaging,[2] we find the energy conversions in the low- and high-latitude states (Fig. 10), and the former conversion pattern is qualitatively similar to the one calculated with respect to the global time average of the flow. In both states, the basin-averaged values of Π and K, that is, Π_{av} and K_{av}, are positive, thus indicating that the fluctuations feed on the mean state. In the low-latitude state, $\Pi_{av} \approx K_{av}$, which indicates that the baroclinic and barotropic instability mechanisms are equally efficient in generating the eddies. However, the former dominates in the return westward flows. In the high-latitude state, Π_{av} increases by 80% and K_{av} increases by 20%. Thus, the high-latitude state generates eddies more efficiently and mostly through the baroclinic instability mechanism. Negative values in the spatial distributions of Π reveal that in the eastward-jet region the fluctuation energy returns to the mean flow, which is consistent with the mean flow rectification driven by the eddy forcing. The negative values of Π are more negative and more confined to the eastward jet in the low- rather than high-latitude state. The spatial distributions of K are more confined to the boundaries, and they exhibit no broad negative regions, thus indicating that fluctuations transfer kinetic energy to the mean.

The importance of the vertical structure of the eddy forcing is addressed by calculating the non-eddy-resolving solutions driven by either f_1' or f_2'. Without the upper-layer eddy forcing, the eastward-jet enhancement does not emerge; hence, this enhancement is mainly an upper-ocean phenomenon. Without the middle-layer eddy forcing, the eastward jet is noticeably exaggerated in the upper layer. This is so because the eddy buoyancy flux fluctuations tend to oppose each other in the first and second layers; hence there is some mutual cancellation between their large-scale responses. Thus, given the coarse and idealized stratification, the vertical structure of the eddy forcing is only moderately important.

The middle-layer flows driven by the eddy-forcing components $\langle f \rangle$, $\langle f_2 \rangle$, f_1', and f_2' are shown in Fig. 11. The $\langle f \rangle$-induced flow, which is noticeable in the northwestern corner of the basin and around the eastward jet, and the f_1'-induced flow are both due to the baroclinic instabilities of the eddy-induced upper-layer circulation patterns. The time-mean gyres of the $\langle f_2 \rangle$-induced flow are the dominant components of the eddy-driven deep-ocean circulation. They are associated with the baroclinic instability that spins down the upper-ocean gyres but spins up the deep ocean. The middle-layer fluctuations of the eddy forcing are relatively small; therefore the rectified flow consists of several zonally elongated recirculation cells (Fig. 11c) rather than a recirculation dipole enhancing the eastward jet

[2] When averaging is conditional, tendency term in the energy equation is generally nonzero, but here it is small and, therefore, neglected.

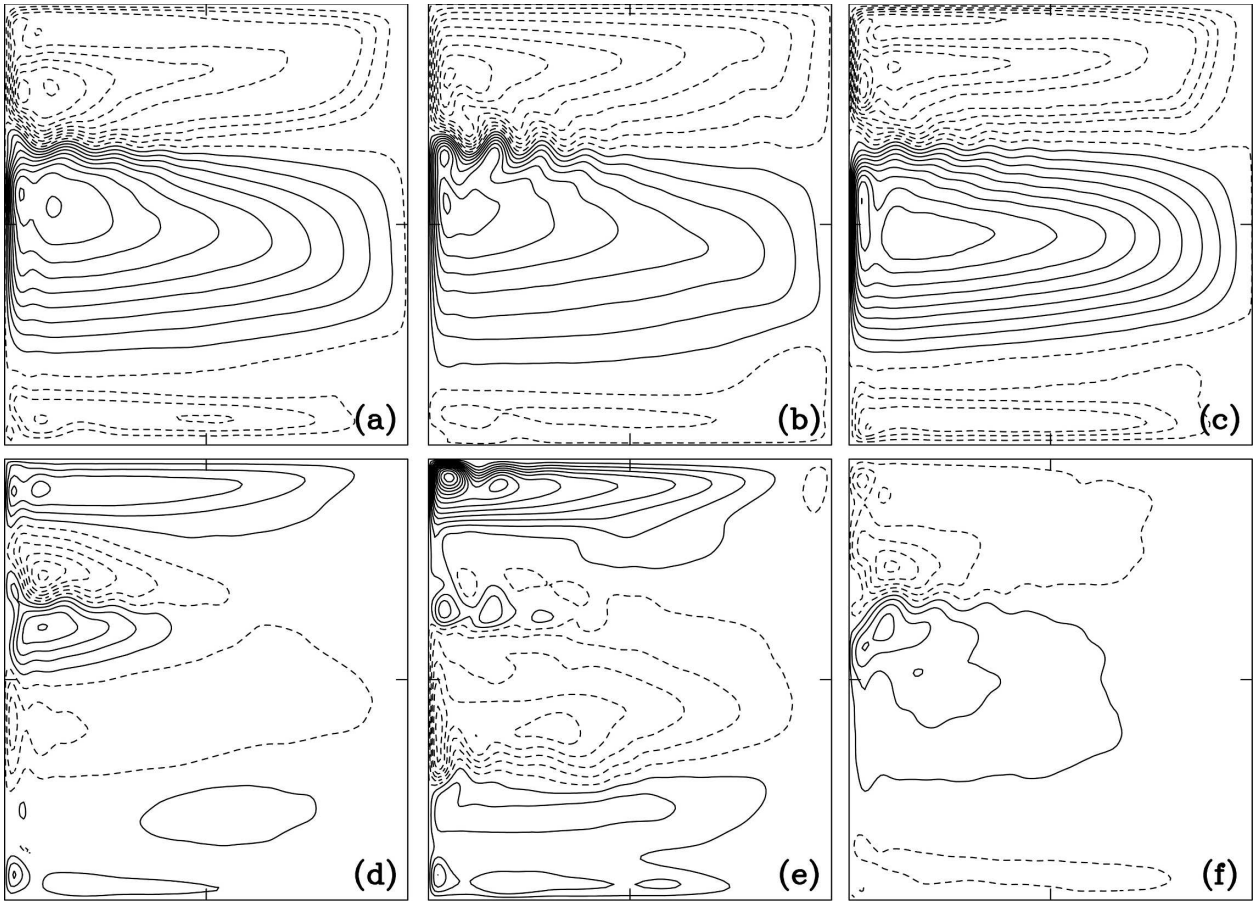

FIG. 7. Effects of the time-mean and fluctuation components of the eddy forcing, with and without the atmospheric forcing. Time-mean, upper-ocean velocity streamfunctions (CI = 3 Sv) of the forced non-eddy-resolving solutions driven by the atmospheric forcing history, W, and by (a) the full (but temporally interpolated) eddy forcing, f_i or by its (b) time-mean $\langle f_i \rangle$ and (c) fluctuation f_i' components. The corresponding solutions driven only by (d) f_i, (e) $\langle f_i \rangle$, and (f) f_i' (i.e., with $W = 0$) are also shown.

(Berloff 2005c). To summarize, the roles of all the eddy inputs are comparable in structuring the middle-layer mean flow.

b. *Dynamical mechanism of the eddy–mean flow interaction*

Fluctuating eddy forcing with zero time mean is capable of driving rectified (i.e., nonzero time mean) large-scale flows, as shown originally in laboratory experiments (Whitehead 1975). Two regimes of rectification are relevant to the double gyres, and both of them result in formation of zonal currents (Rhines 1975, 1994). Consider the potential vorticity dynamics forced by localized zero-mean external forcing, $\Phi(t, \mathbf{x})$, with positive amplitude A:

$$\frac{dq}{dt} + \beta v = A\Phi(t, \mathbf{x}). \tag{16}$$

Integrating (16) over a short time and multiplying by the flow velocity yields

$$\delta q v = (A \int \Phi \, dt - \beta \delta y) v. \tag{17}$$

At the latitudes outside of the localized forcing, taking into account that $v = \delta y/\delta t$ and averaging over an ensemble of realizations (denoted by angular brackets) reveals

$$\langle \delta q v \rangle = -\frac{\beta}{2} \frac{d}{dt} \langle y^2 \rangle. \tag{18}$$

Assuming irreversible[3] Lagrangian dispersion implies the asymptotic diffusive limit, in which $\langle y^2 \rangle \sim t$. In this limit, the rhs of (18) is negative; hence, the ensemble-

[3] True irreversibility requires some mixing at the end of the enstrophy cascade.

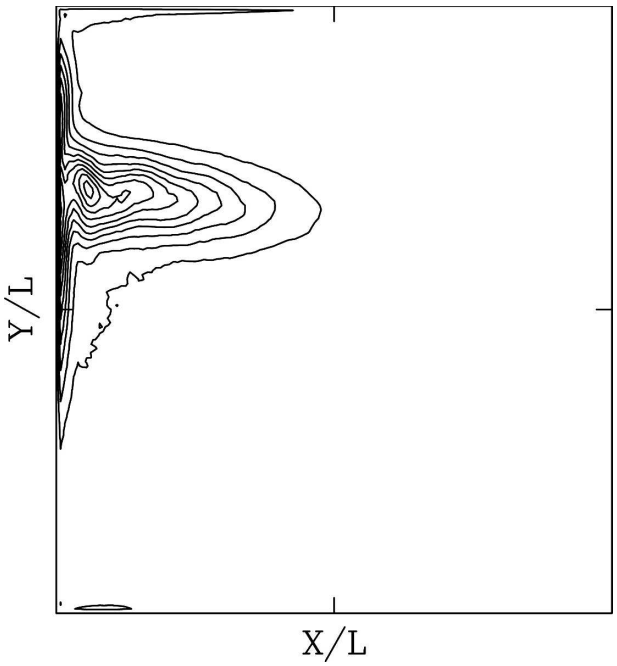

FIG. 8. Spatial distribution of the upper-ocean eddy-forcing variance, $\sqrt{\sigma(f_1)}$ (CI = 0.5×10^{-10} s^{-2}).

average meridional flux of q, which is equivalent to the Eulerian flux of q, is negative. This flux results in the westward acceleration of the background ensemble-average flow, as can be seen from the zonally averaged vorticity equation:

$$\frac{\partial \overline{u}^x}{\partial t} = \overline{qv}^x. \tag{19}$$

The resulting flow regime is due to the meridional mixing and partial homogenization of the absolute potential vorticity.

The second regime occurs when the forcing is sufficiently strong and $v\langle\int \Phi\, dt\rangle > 0$, which is a typical phenomenon for the β-plane dynamics (16) in the near-Sverdrup regime. An argument for the positive correlation is the necessity to have a countercurrent that closes the westward current and enforces the conservation of mass. Thus, in the second regime the meridional q flux is positive; hence, it drives the eastward background current. An alternative explanation (Thompson 1971) is that eastward jet is driven by convergence of the Reynolds stress associated with Rossby waves radiating away from the forced latitudes.

In the double-gyre ocean, both regimes are present simultaneously because the eddy forcing is strong around the eastward-jet axis but weak elsewhere. Therefore, the rectified flow response consists of the cyclonic/anticyclonic recirculations to the north/south of the eastward jet. The underlying eddy/mean flow interaction is characterized by the following ingredients. First, as suggested by the energy conversion arguments (section 3a), the eddies are generated by instabilities in the western boundary currents and the upstream part of their eastward-jet extension. Then, the eddies are advected downstream by the background flow. Along the eastward jet, and particularly near its eastern end,[4] the eddies backscatter into the enhancement of the large-scale eastward jet and its adjacent recirculation zones through the rectification mechanism described above.

It is useful to compare the double-gyre eastward-jet dynamics with the classical situation of a zonal, baroclinically unstable eastward jet (e.g., Vallis 2006). In the latter case, the time-averaged equation for the enstrophy, $E' = q'^2/2$, can be written as

$$\frac{\partial \overline{E'}}{\partial t} + \frac{\partial \langle u\rangle\langle E'\rangle}{\partial x} + \frac{\partial \langle v\rangle\langle E'\rangle}{\partial y} + \langle u'q'\rangle\frac{\partial\langle q\rangle}{\partial x} + \langle v'q'\rangle\frac{\partial\langle q\rangle}{\partial y} + \frac{\partial\langle u'E'\rangle}{\partial x} + \frac{\partial\langle v'E'\rangle}{\partial y} = -\langle D'q'\rangle, \tag{20}$$

where D' represents dissipation, and angular brackets and prime denote conventional definitions of the time mean and fluctuations around it. In the stationary case, the tendency term disappears. Zonal averaging of (20) removes the x derivatives, and an additional integration in the meridional direction yields

$$\int\int \left(\langle D'q'\rangle + \langle v'q'\rangle\frac{\partial\langle q\rangle}{\partial y}\right) dx\, dy = 0. \tag{21}$$

In the above integral balance, the first term is positive; therefore, the second term must be negative. This implies that eddy PV flux is downgradient in the integral sense, which is also true in a closed basin. On the other hand, the downgradient property of the eddy flux is not necessarily true locally, because advection of the enstrophy enters the balance.

c. Role of the eddies in the low-frequency variability

Given that nonlinear adjustment of the oceanic eastward jet is an essential part of the coupled variability (Kravtsov 2007), and that the jet is driven mainly by the eddy-forcing fluctuations, we have made a low-frequency analysis of the eddy-forcing variance in order to relate that variance to the evolving large-scale flow. With that in mind, the total eddy forcing is decomposed

[4] We have checked this statement with the eddy-corrected non-eddy-resolving model, by calculating large-scale flow responses to additional, spatially localized patches of the eddy forcing introduced at different locations along the eastward-jet axis.

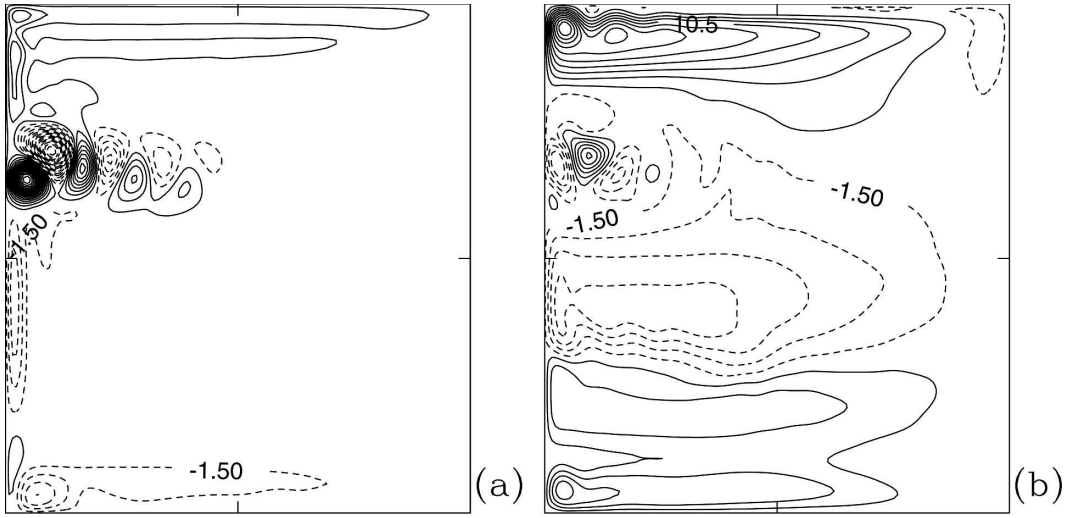

FIG. 9. Roles of the vorticity and buoyancy eddy forcings. Time-mean, upper-ocean velocity streamfunctions of the non-eddy-resolving solutions forced only by (a) the relative vorticity $\langle R_i \rangle$ and (b) buoyancy $\langle B_i \rangle$ components of the time-mean eddy forcing (CI = 3 Sv).

into low-passed and residual high-passed fluctuations, respectively,

$$f_i(t, \mathbf{x}) = f_i^{\mathrm{LP}}(t, \mathbf{x}) + f_i^{\mathrm{HP}}(t, \mathbf{x}), \tag{22}$$

as defined by a 1000-day running average. The high-passed fluctuations are characterized by their finite-time variance, $\sigma(f_i)^{\mathrm{HP}}(t, x, y)$, calculated over the same time interval. The spatial structure and temporal variability of $\sigma(f_i)^{\mathrm{HP}}$ are described in terms of the EOFs and their principal components (Fig. 12). Most of the low-frequency variability is captured by the first EOF. The corresponding principal component is strongly correlated (correlation coefficient is $C \approx 0.8$) with the first oceanic EOF principal component of the reference solution (section 2a). The spatial pattern of the leading EOF of the eddy-forcing variance describes the dramatic reduction of the variance associated with ocean transitions to the high-latitude state. This reduction occurs because the low-latitude state is characterized by the least energetic currents, due to the change of the Ekman pumping pattern. The second EOF corresponds to the coherent north–south shifts of the variance, and its principal component is weakly but noticeably ($C \approx 0.3$) correlated with the second and third oceanic EOF principal components.

To characterize the reference solution and simply relate the eddy-forcing variance and the large-scale flow, the following indices are defined and calculated: I_{BT}^{A}, I_{BC}^{O}, I_{BT}^{O}, and I_{L1}^{f}. Here, the superscript indicates whether the index describes the ocean (O), the atmosphere (A), or the ocean eddy forcing (f), and the subscripts refer to the barotropic-mode streamfunction (BT), oceanic baroclinic streamfunction, $\psi_{\mathrm{BC}} = \psi_1 - \psi_2$ (BC), or the top oceanic isopycnal layer (L1). Index I_{BT}^{A} is nondimensional latitude of the maximum of zonally averaged, barotropic zonal velocity, and it is found by cubic interpolation. Index I_{L1}^{f} is found similarly, but for the nondimensional latitude of the maximum amplitude of the eddy-forcing fluctuations. The indices I_{BC}^{O} and I_{BT}^{O} are found by averaging the corresponding streamfunctions over the middle ⅔ of the basin (i.e., without the basin margins near the zonal boundaries), and then by removing the means from the resulting time series. All indices are normalized by their variances. The time-lag correlation function between any two indices I_1 and I_2 is defined as

$$C(I_1, I_2)(\tau) = \frac{[I_1(t) - \langle I_1 \rangle][I_2(t + \tau) - \langle I_2 \rangle]}{\sqrt{\sigma_1 \sigma_2}}, \tag{23}$$

where σ_1 and σ_2 are the corresponding variances.

The low-frequency variability of the ocean appears most clearly in I_{BC}^{O}, whereas I_{BT}^{O} is highly correlated with the atmosphere [$C(I_{\mathrm{BT}}^{O}, I_{\mathrm{BT}}^{A}) = 0.9$] and, therefore, noisy. The difference between these indices is set by the difference between the fast barotropic and slow baroclinic ocean adjustments to variable atmospheric forcing. Index I_{BC}^{O} lags I_{BT}^{A} by a few years, with high correlation,[5] and it is also strongly correlated with I_{L1}^{f} at zero

[5] Technically, the time lag can be reduced and the correlation maximum can be enhanced by considering another atmospheric index, which is given by the time average of I_{BT}^{A} from some time in the past to the current time.

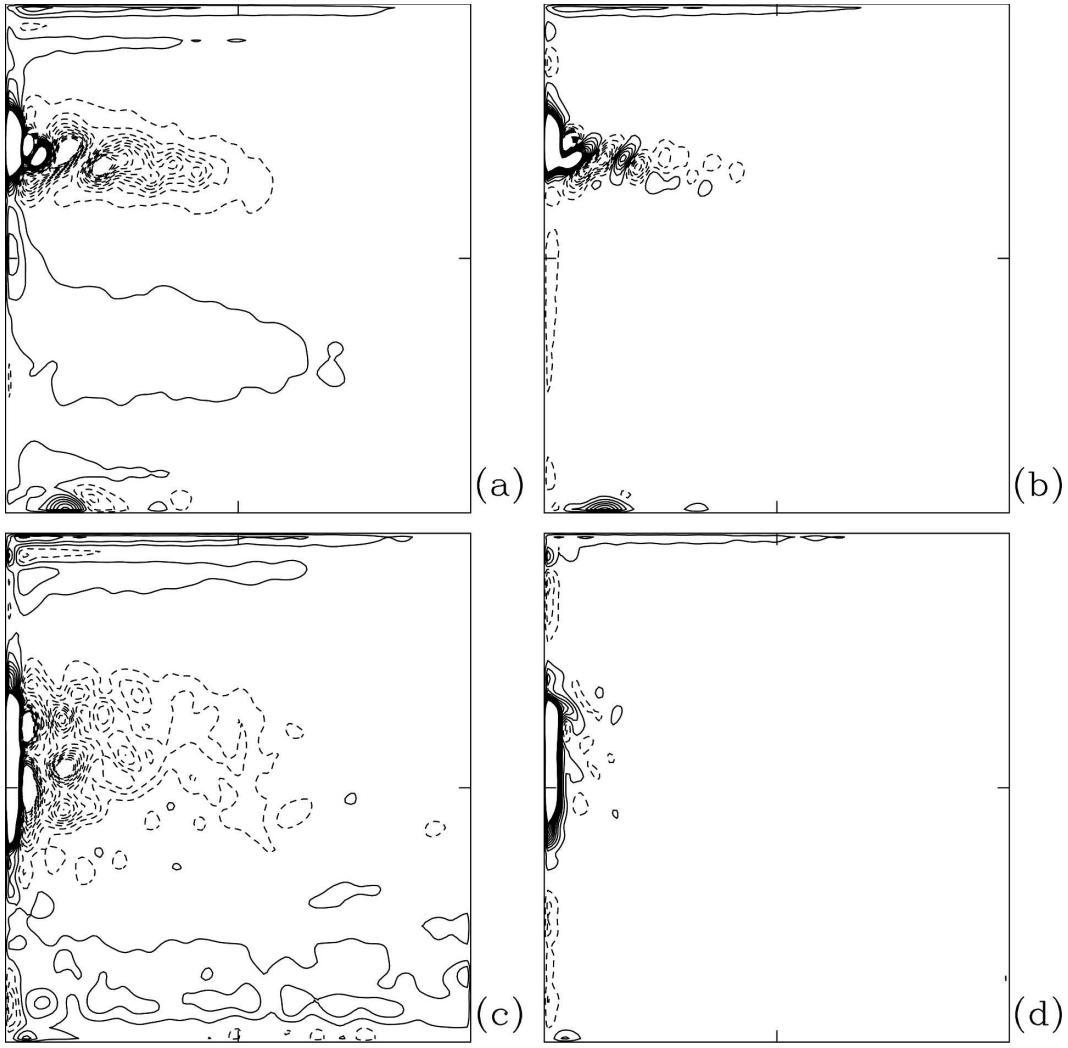

FIG. 10. Conditionally averaged (a) potential $\Pi(x, y)$ and (b) kinetic $K(x, y)$ energy conversion terms in the low-latitude state. (c), (d) Same quantities as in (a), (b) but for the high-latitude state. All the fields are normalized by their average values (CI = 5).

lag. The latter correlation is high because I^O_{BC} reflects variation of the potential energy storage that feeds the eddies. In summary, the above observations make the basis for relating the eddy-forcing variance to I^O_{BC}—this is the basis for the parameter closure developed in section 4.

4. Eddy parameterization in a coupled model

In this section, fluctuations of the eddy forcing f' that play a crucial role in driving the large-scale climatology and low-frequency variability, are modeled in terms of a random process. First, we assume that the variance of f' is stationary and given by (10). Then, we estimate the temporal and spatial correlation functions of f. From the former we find the integral correlation time,

$$T_i^{\mathrm{INT}}(\mathbf{x}) = \sigma(f_i)^{-1}(x, y) \int_0^\infty \langle f_i'(t, x, y) f_i'(t + \tau, x, y) \rangle \, d\tau, \tag{24}$$

and the horizontal correlation function,

$$R_i^{\mathrm{HOR}}(x, y; x_0, y_0) = \frac{\langle f_i'(t, x_0, y_0) f_i'(t, x, y) \rangle}{\sigma(f_i)^{1/2}(x_0, y_0) \sigma(f_i)^{1/2}(x, y)}. \tag{25}$$

Around the western boundary current and the eastward jet, T_i^{INT} varies from 5 to 10 days and R^{HOR} monotonically decays to zero over about 100 km. The low-frequency variations of R^{HOR} and T^{INT} are weak, unlike those of the variance (section 3c); therefore we treat

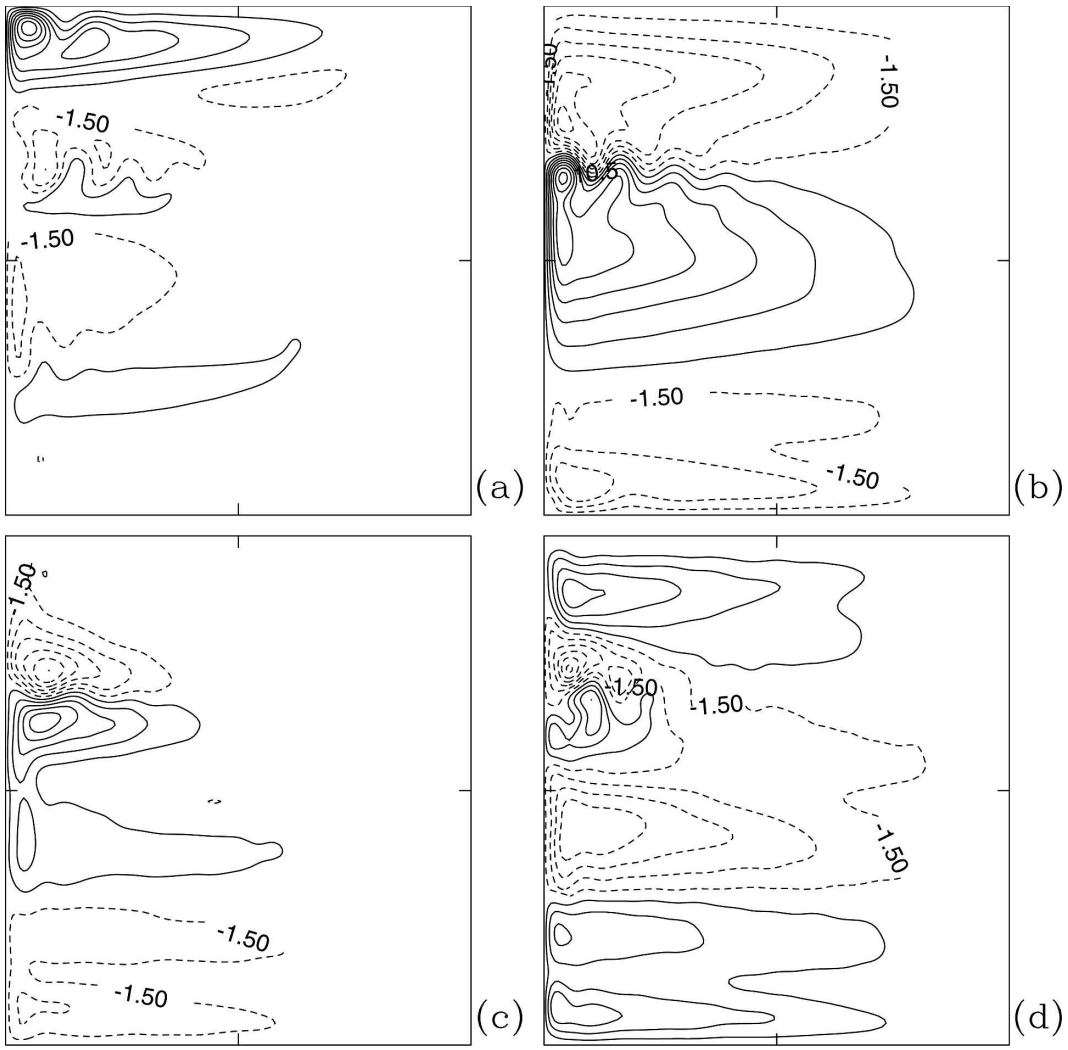

FIG. 11. Middle-layer dynamic response to the eddy forcing. Time-mean, middle-layer velocity streamfunctions (CI = 3 Sv) of the non-eddy-resolving solutions forced by different time mean and fluctuation components of the eddy forcing: (a) $\langle f_1 \rangle$, (b) $\langle f_2 \rangle$, (c) f_1', and (d) f_2'. The roles of all the eddy inputs are comparable in structuring the middle-layer mean flow.

both of these quantities as stationary but spatially inhomogeneous.[6]

Details of a random-forcing model of the eddies that is embedded into the non-eddy-resolving ocean model are in the appendix. First, we computed a randomly forced coupled solution (not shown) with the stationary but spatially inhomogeneous eddy-forcing variance, $\sigma(f_i)$, defined in (10) and shown in Fig. 8. Because nonlinear rectification mechanism is activated by the random forcing, this solution has a well-developed time-mean oceanic eastward jet. However, it exhibits no transitions of the ocean to the high-latitude state. This undesirable behavior is reflected in the history of the oceanic eastward-jet index, EJ $- I^O_{\mathrm{L1}}$, which is calculated as the latitude of the maximum eastward, zonally averaged flow velocity. This index exhibits no transitions to the low-latitude state, unlike in the reference solution.

The modeling failure resulting from the stationary treatment of the eddy-forcing variance can be overcome by taking into account its low-frequency variability. This is achieved by relating the eddy-forcing structure to the interactively calculated I^O_{BC}. (The adopted approach is simple, and an elaborate extension of it can be made by replacing I^O_{BC} with projection of the flow solution on the leading EOF shown in Fig. 4.) The cor-

[6] Also, we find that both R^{HOR} and T^{INT} can be successfully approximated as horizontally homogeneous parameters, by imposing their averages in the eastward-jet region.

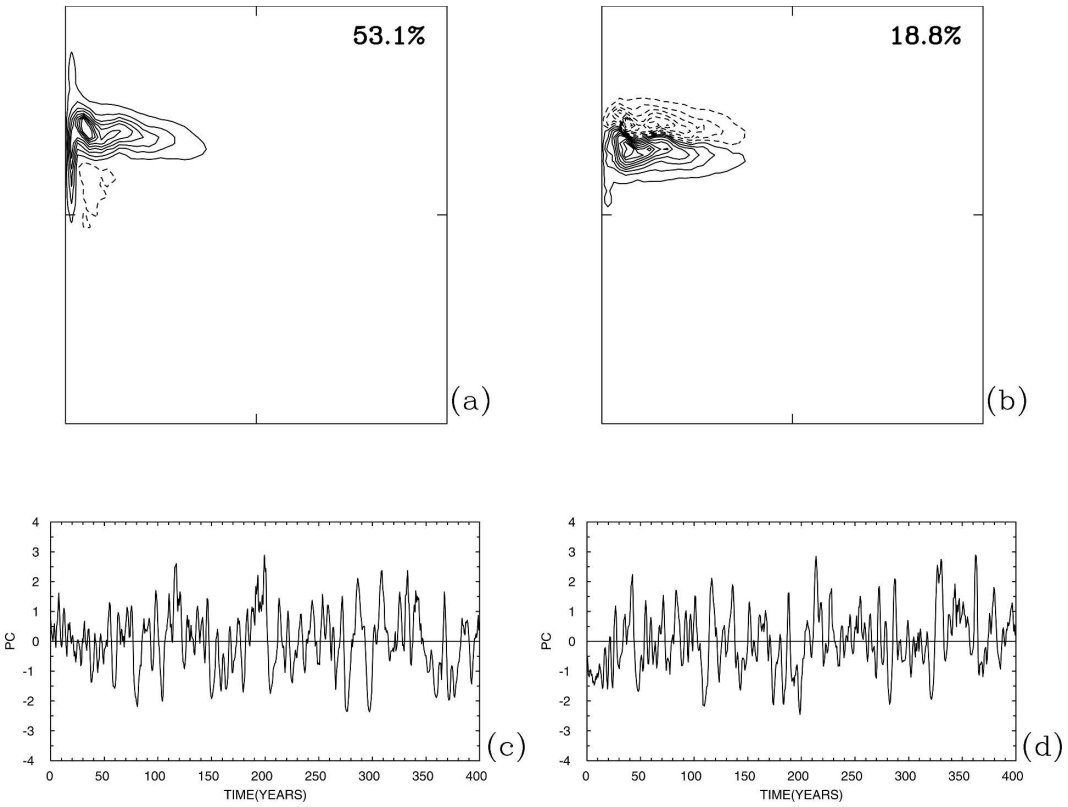

FIG. 12. Low-frequency variability of the eddy forcing. Leading EOFs of the high-passed upper-ocean eddy-forcing variance: (a) the first and (b) the second EOFs. The corresponding principal components are shown in (c) and (d), respectively. The corresponding fractions of the total variance are indicated in terms of percentage. The EOFs are normalized by their maximum absolute values (CI = 0.1), and the principal components are normalized by their variances, respectively.

responding relationship is found in terms of the conditional time averaging of f with respect to $I^O_{\rm BC}$ of the reference solution. The outcome is a set of conditional averages, $\{f_i\}_m$, with $m = 1, \ldots, M$, where we choose $M = 10$. Here, $\{\}_m$ indicates integration over the corresponding time intervals weighted by their total length (i.e., the ensemble average). The set of M conditional eddy-forcing variances,

$$\sum_m (f_i) = \{(f_i - \{f_i\}_m)^2\}_m, \tag{26}$$

is found with two rounds of averaging. The corresponding M bands of $I^O_{\rm BC}$ (Table 2) are chosen so that, on the one hand, each $\Sigma_m(f_i)$ is based on a substantial number of events, but, on the other hand, M is not small and permits a sensitivity study. Here, it is found that the results do not change qualitatively with $M = 5$. The corresponding set of the eddy-forcing averages and variances (Fig. 13) can be viewed as a simple *parameter closure* that relates random forcing and oceanic large-scale flow. The random forcing can be formally expressed as

$$f_i(t,x,y) = \{f_i\}_m[x,y;I^O_{\rm BC}(t)] + f_i'\left(t,x,y;\sum_m [x,y;I^O_{\rm BC}(t)]\right). \tag{27}$$

Here, the functional dependences on $I^O_{\rm BC}$, which are calculated interactively, are given by the M discrete states; and random f_i' field is found for the given variance [unlike in (26) where the variance itself is found

TABLE 2. Relationship table between the σ_f index and minimum and maximum limits of the corresponding zonal band of the $I^O_{\rm BC}$ index.

σ_f index	Min position	Max position
1		−4.8
2	−4.8	−4.1
3	−4.1	−2.9
4	−2.9	−2.5
5	−2.5	−1.6
6	−1.6	0.0
7	0.0	0.5
8	0.5	0.7
9	0.7	0.9
10	0.9	

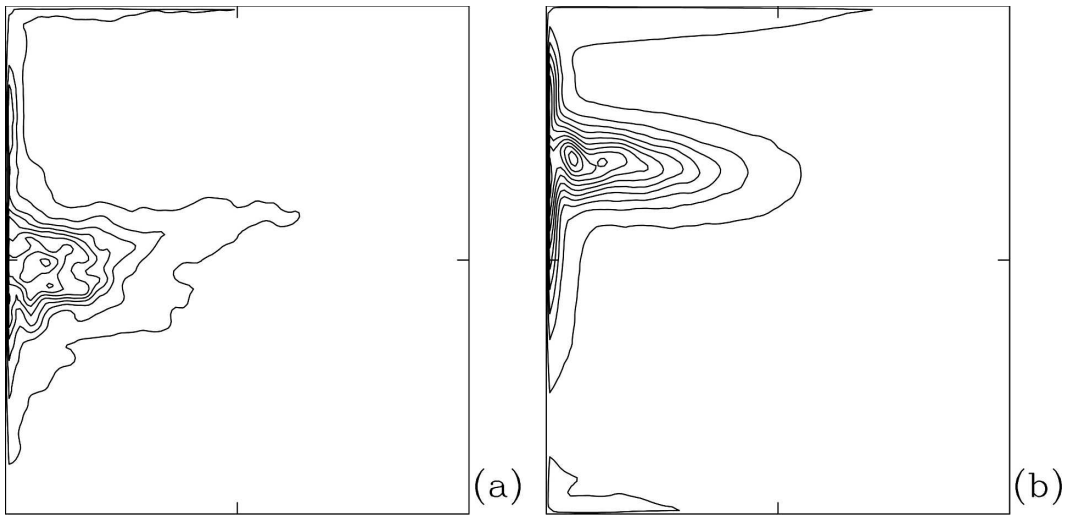

FIG. 13. Spatial distributions of the upper-ocean conditional eddy-forcing variance, $\sqrt{\Sigma_m(f_1)}$, in (a) the high-latitude state with index $m = 1$ and (b) the low-latitude state with index $m = 8$ (CI = 0.5×10^{-10} s^{-2}).

diagnostically]. Thus, the random forcing can be classified as a multiplicative noise (e.g., Majda et al. 1999), because it depends on the state of the large-scale flow. Last, since the ocean model response to f_i' is more important than that to $\{f_i\}_m$, we focus on the fluctuation variance.

The coupled-model dynamics with the random-forcing variance related to the oceanic eastward-jet index, EJ $- I^O_{\mathrm{L1}}$, is analyzed in terms of the climatology, statistical indices, and EOF patterns of its solution. Unlike in the stationary-forcing case, EJ $- I^O_{\mathrm{L1}}$ exhibits the transitions to the high-latitude state characteristic of the reference solution. Other features of the randomly forced solution also exhibit skill in reproducing the reference solution (Fig. 14). Because of the eddy forcing, the flow has a well-developed eastward jet, and, because of the nonstationarity of the variance, it exhibits decadal low-frequency variability. The latter is indicated by the extreme negative events of the leading EOF principal component (Fig. 15). Spatial patterns of the leading EOFs are similar to those of the reference solution (Fig. 4). The variance of the leading EOF principal component is about 10% smaller than that of the reference solution, likely reflecting the pair of particularly strong events in the latter (at about 280 and 300 yr). On the negative side, in the randomly forced solution the oceanic eastward jet is less sharp than in the reference solution; therefore some additional information about space–time correlation structure of the eddy forcing has to be taken into consideration for further refinement of the eddy parameterization. The second and third EOF principal components have less frequent extreme events than in the reference solution, and, perhaps, this can be attributed to their spatial structure that has a weaker footprint of the eastward jet.

5. Summary

The role of oceanic mesoscale eddies is analyzed in a quasigeostrophic, midlatitude, coupled ocean–atmosphere model operating at large Reynolds number (Kravtsov et al. 2007, 2007). The model dynamics are characterized by decadal variability that involves nonlinear adjustment of the ocean to coherent north–south shifts of the atmosphere. An important point is that both the oceanic climatology and adjustment are controlled by the mesoscale oceanic eddies, and the eddy-induced sea surface temperature anomalies feed back on the atmosphere. If the eddies are parameterized in terms of eddy viscosity, the coupled variability is suppressed (Kravtsov et al. 2006). This is because the eddy effects are not viscous, and our goal is to understand and parameterize them.

The oceanic eddies are diagnosed by the dynamical decomposition method of Berloff (2005a) adapted for nonstationary atmospheric forcing. The corresponding eddy-forcing history is added to a non-eddy-resolving ocean model, thus allowing for dynamical interpretation of the eddy effects. In particular, it is found that the main effects of the eddies are (i) enhancement of the oceanic eastward jet separating the subpolar and subtropical gyres and (ii) weakening of the gyres. The enhancement is due to the nonlinear flow rectification in the presence of the background planetary vorticity gradient. The rectification is driven by spatially localized, temporal fluctuations of the upper-ocean eddy forcing. This is a nonlocal process involving generation of the

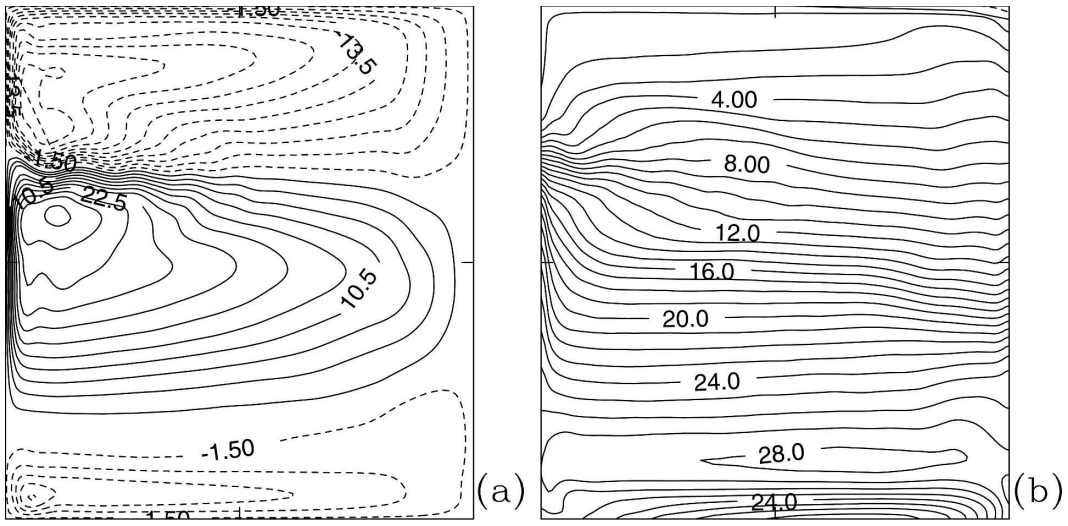

FIG. 14. Climatology of the randomly forced coupled solution: (a) $\langle \psi_1 \rangle$ (CI = 3 Sv), and (b) the time-mean sea surface temperature (CI = 1°C).

eddies by the flow instabilities in the western boundary current and the upstream part of the eastward jet. The energized eddies are advected by the mean flow to the east, where they backscatter into the rectified enhancement of the eastward jet. The flow-weakening effect, which is due to the time-mean buoyancy component of the eddy forcing, is a result of the baroclinic instability of the westward return currents.

Eventually, we parameterize the deterministic eddy-forcing history as a random-forcing process acting within the non-eddy-resolving ocean model (Berloff 2005b). The random forcing is characterized by variance, and space and time correlations, and here the novel aspect is that these properties are nonstationary because of the low-frequency coupled variability. The stochastic approach advocated here is an alternative to the more common approach of parameterizing the eddies in terms of eddy viscosity. At this point, the main advantage of the random-forcing model is that it captures the antiviscous, eddy-induced rectification, which is here the key dynamical process.

Following the proposed strategy, spatially inhomogeneous parameters of the random process are diagnosed from the reference eddy-resolving solution. At that point the eddy-resolving data are used as a replacement for the actual observations. It is found that because of the decadal variability, the forcing variance has to be treated as not only inhomogeneous but nonstationary, while all other parameters can be treated as stationary. The forcing variance is related to baroclinicity of the ocean state—this is a simple parameter closure of the random-forcing model. Last, a model run with the random forcing yields correct climatology and low-frequency variability in the non-eddy-resolving coupled solution.

The following extensions of the presented results are anticipated within intermediate-complexity coupled modeling. Ocean eddy dynamics of other regimes have to be explored (e.g., Hogg et al. 2005, 2006) in order to identify the most generic behaviors. Also, findings of this paper remain to be verified in less idealized models. An alternative to the non-eddy-resolving ocean model can be a severely truncated model based on a few empirical orthogonal functions (Franzke et al. 2005; Kravtsov et al. 2005). Attempts to localize the relationship between the random-forcing variance and the ocean state have to be made by accounting for pointwise correlations between the large-scale flow and the eddy forcing. However, our results suggest that the parameterization cannot be made fully local. Also, some refinement can be done by incorporating more of the eddy-forcing statistics into the random model. The approach discussed here represents a first step toward parameterizing eddy effects in a dynamically consistent way in coarse-resolution, comprehensive, general circulation coupled climate models.

Acknowledgments. Comments from Michael Ghil are gratefully acknowledged. Suggestions made by anonymous reviewers also led to significant improvement of this work. Funding for this work came from NSF Grants OCE 02-221066 and OCE 03-44094. Additional funding for PB was provided by the U.K. Royal Society Fellowship and by WHOI Grants 27100056 and 52990035. Also, Ms. S. Elsner is gratefully acknowledged for assistance in manuscript preparation.

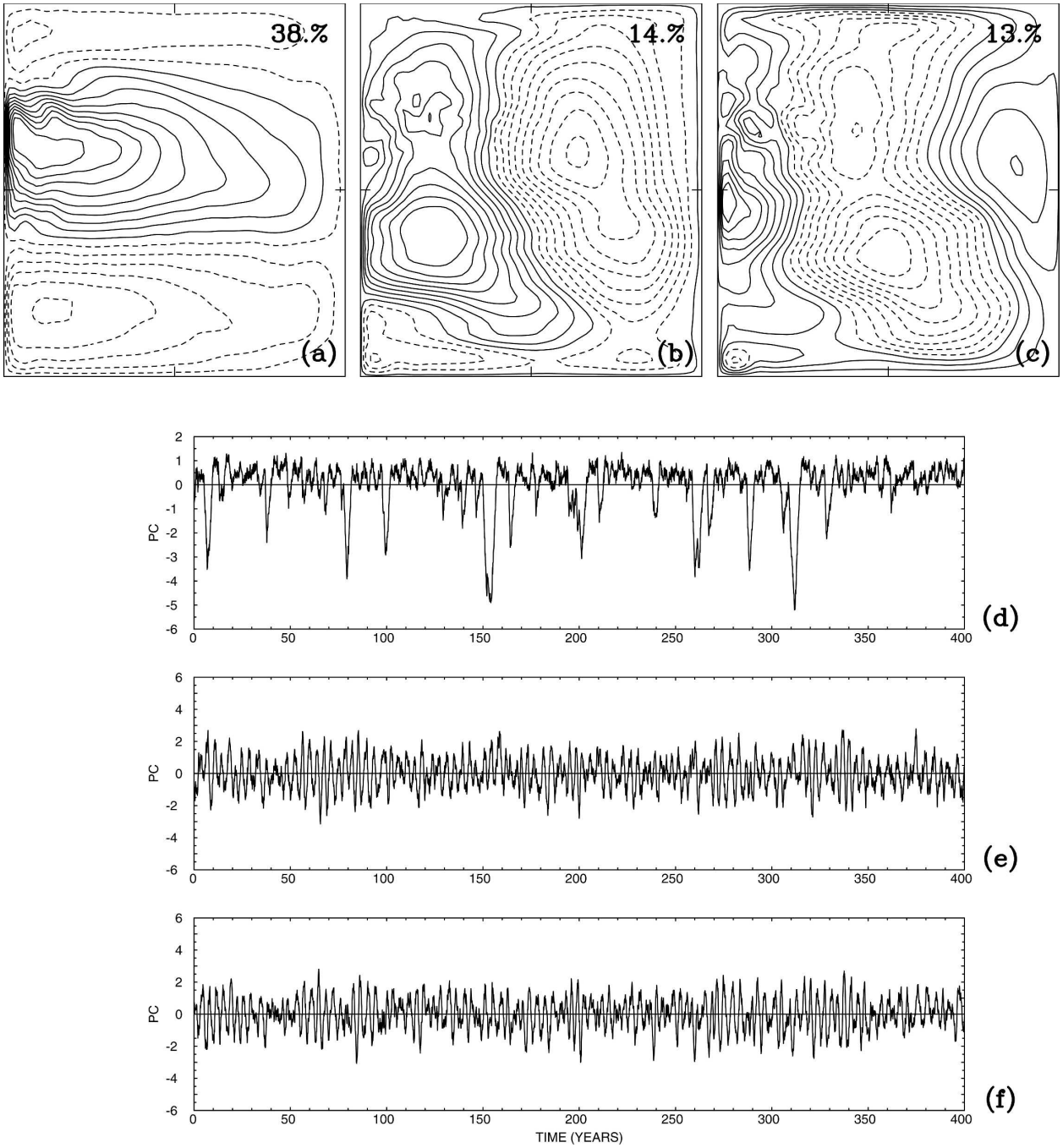

FIG. 15. Same as Fig. 4, but for the randomly forced solution.

APPENDIX

Random-Forcing Model

A random-forcing model of the eddies is constructed and embedded into the non-eddy-resolving ocean model as follows. A unit variance forcing vector is generated by the first-order autoregressive process,

$$\mathbf{g}(t) = \exp(-dt/T^{\mathrm{INT}})\mathbf{g}(t - dt) + \mathbf{dW}, \qquad \text{(A1)}$$

where **dW** is a random increment vector (Wiener process), and dt is the non-eddy-resolving model time step. The elements of the vector **g** correspond to different grid nodes, and they are mutually uncorrelated. These elements are transformed to mutually correlated elements by the transformation matrix **L**:

$$\mathbf{f}(t) = \mathbf{L}\mathbf{g}(t). \qquad \text{(A2)}$$

The **L** is found from the correlation matrix for **f**,

$$\mathbf{C} = \langle \mathbf{f}\mathbf{f}^{\mathrm{T}} \rangle, \tag{A3}$$

which has elements given by (25) and is simply related to $\mathbf{L}$:

$$\mathbf{C} = \mathbf{L}\mathbf{L}^{\mathrm{T}}. \tag{A4}$$

The transformation matrix is calculated from $\mathbf{C}$ with a factorization algorithm [here we use the Cholesky algorithm (Press et al. 1992)]. Once $\mathbf{f}$ is obtained from (A2), it is multiplied by the square root of the spatially inhomogeneous eddy-forcing variance.

Vertical correlations of the eddy forcing are found to be only moderately important; hence they are neglected. The algorithm is used to generate forcing at the coarse-grid nodes belonging to the basin subdomain in which the upper-ocean, $\sqrt{\sigma(f_1)}$, exceeds 0.5×10^{-10} s^{-2} [this is 10% of the maximum value of $\sqrt{\sigma(f_1)}$]. The corresponding sensitivity study showed that the solution does not change significantly with a larger subdomain. Explicit fluctuations of the deep-ocean eddy forcing are neglected for simplicity, and their net effect is modeled by a 20% reduction of the upper-ocean $\sqrt{\sigma(f_1)}$, in accordance with findings of section 3a.

REFERENCES

Berloff, P., 2005a: On dynamically consistent eddy fluxes. *Dyn. Atmos. Oceans,* **38,** 123–146.

——, 2005b: Random-forcing model of the mesoscale oceanic eddies. *J. Fluid Mech.,* **529,** 71–95.

——, 2005c: On rectification of randomly forced flows. *J. Mar. Res.,* **31,** 497–527.

——, and J. C. McWilliams, 1999: Large-scale, low-frequency variability in wind-driven ocean gyres. *J. Phys. Oceanogr.,* **29,** 1925–1949.

Deser, C., and M. Blackmon, 1993: Surface climate variations over the North Atlantic Ocean during winter: 1900–1989. *J. Climate,* **6,** 1743–1753.

Dewar, W., 2003: Nonlinear midlatitude ocean adjustment. *J. Phys. Oceanogr.,* **33,** 1057–1081.

Feliks, Y., M. Ghil, and E. Simonnet, 2004: Low-frequency variability in the midlatitude atmosphere induced by an oceanic thermal front. *J. Atmos. Sci.,* **61,** 961–981.

Franzke, C., A. Majda, and E. Vanden-Eijnden, 2005: Low-order stochastic mode reduction for a realistic barotropic model climate. *J. Atmos. Sci.,* **62,** 1722–1745.

Goodman, J., and J. Marshall, 1999: A model of decadal middle-latitude atmosphere–ocean interaction. *J. Climate,* **12,** 621–641.

Haidvogel, D., and P. Rhines, 1983: Waves and circulation driven by oscillatory winds in an idealized ocean basin. *Geophys. Astrophys. Fluid Dyn.,* **25,** 1–63.

Herring, J., and R. Kraichnan, 1971: Comparison of some approximations for isotropic turbulence. *Statistical Models and Turbulence,* M. Rosenblatt and C. van Atta, Eds., Springer-Verlag, 147–194.

Hogg, A., W. Dewar, P. Killworth, and J. Blundell, 2003: A quasi-geostrophic coupled model: Q-GCM. *Mon. Wea. Rev.,* **131,** 2261–2278.

——, P. Killworth, J. Blundell, and W. Dewar, 2005: Mechanisms of decadal variability of the wind-driven ocean circulation. *J. Phys. Oceanogr.,* **35,** 512–531.

——, W. Dewar, P. Killworth, and J. Blundell, 2006: Decadal variability of the midlatitude climate system driven by the ocean circulation. *J. Climate,* **19,** 1149–1166.

Holland, W., 1978: The role of mesoscale eddies in the general circulation of the ocean—Numerical experiments using a wind-driven quasigeostrophic model. *J. Phys. Oceanogr.,* **8,** 363–392.

Holm, D., and B. Nadiga, 2003: Modeling mesoscale turbulence in the barotropic double-gyre circulation. *J. Phys. Oceanogr.,* **33,** 2355–2365.

Kravtsov, S., D. Kondrashov, and M. Ghil, 2005: Multilevel regression modeling of nonlinear processes: Derivation and applications to climatic variability. *J. Climate,* **18,** 4404–4424.

——, P. Berloff, W. Dewar, M. Ghil, and J. McWilliams, 2006: Dynamical origin of low-frequency variability in a highly nonlinear midlatitude coupled model. *J. Climate,* **19,** 6391–6408.

——, W. Dewar, P. Berloff, J. McWilliams, and M. Ghil, 2007: A highly nonlinear coupled mode of decadal variability in a mid-latitude ocean-atmosphere model. *Dyn. Atmos. Oceans,* in press.

Kushnir, Y., 1994: Interdecadal variations in North Atlantic sea surface temperature and associated atmospheric conditions. *J. Climate,* **7,** 141–157.

Latif, M., and T. Barnett, 1994: Causes of decadal climate variability in the North Pacific/North Atlantic sector. *Science,* **266,** 634–637.

Laval, J.-P., B. Dubrulle, and J. C. McWilliams, 2003: Langevin models of turbulence: Renormalization group, distant interaction algorithms or rapid distortion theory? *Phys. Fluids.,* **15,** 1327–1339.

Majda, A., I. Timofeyev, and E. Vanden Eijnden, 1999: Models for stochastic climate prediction. *Proc. Natl. Acad. Sci. USA,* **96,** 14 687–14 691.

McWilliams, J., 1977: A note on a consistent quasi-geostrophic model in a multiply connected domain. *Dyn. Atmos. Oceans,* **1,** 427–441.

Pierce, D., T. Barnett, N. Schneider, R. Saravanan, D. Dommenget, and M. Latif, 2001: The role of ocean dynamics in producing decadal climate variability in the North Pacific. *Climate Dyn.,* **18,** 51–70.

Preisendorfer, R., 1988: *Principal Component Analysis in Meteorology and Oceanography*. Elsevier, 425 pp.

Press, W., B. Flannery, S. Teukolsky, and W. Vetterling, 1992: *Numerical Recipes*. Cambridge University Press, 963 pp.

Rhines, P., 1975: Waves and turbulence on a β-plane. *J. Fluid Mech.,* **69,** 417–443.

——, 1994: Jets. *Chaos,* **4,** 313–339.

Starr, V., 1968: *Physics of Negative Viscosity Phenomena*. McGraw-Hill, 256 pp.

Taylor, G., 1921: Diffusion by continuous movement. *Proc. London Math. Soc.,* **20,** 196–212.

Thompson, R., 1971: Why there is an intense eastward current in the North Atlantic but not in the South Atlantic? *J. Phys. Oceanogr.,* **1,** 235–237.

Vallis, G., 2006: *Atmospheric and Oceanic Fluid Dynamics*. Cambridge University Press, 745 pp.

Wallace, J., 2000: North Atlantic Oscillation/annular mode: Two paradigms–one phenomenon. *Quart. J. Royal Meteor. Soc.,* **126,** 791–805.

Whitehead, J., 1975: Mean flow generated by circulation on a beta-plane: An analogy with the moving flame experiment. *Tellus,* **27,** 358–364.